Article

Not peer-reviewed version

Ribifolones A–H, New Macrocyclic Diterpenes from *Jatropha ribifolia*, their Cytotoxic Activity and Insights Supported by Network Pharmacology and Molecular Modeling

Thalisson Amorim de Souza , Alan Ferreira Alves , Ramon Ramos Marques de Souza , Ana Carolina Ferreira de Albuquerque , Thiago Araújo de Medeiros Brito , Marianna V. Sobral , Fernando Martins dos Santos Junior , Maria de Fátima Agra , Luciana Scotti , Lucas Silva Abreu * , Marcus Tullius Scotti * , Josean Fechine Tavares * , Marcelo Sobral da Silva

Posted Date: 23 March 2026

doi: 10.20944/preprints202603.1635.v1

Keywords: terpenoids; target deconvolution; antiproliferative compounds

 doi:10.20944/preprints202603.1635.v1

Article

Ribifolones A–H, New Macrocyclic Diterpenes from *Jatropha ribifolia*, their Cytotoxic Activity and Insights Supported by Network Pharmacology and Molecular Modeling

Thalisson Amorim de Souza [1], Alan Ferreira Alves [1], Ramon Ramos Marques de Souza [1], Ana Carolina Ferreira de Albuquerque [2], Thiago Araújo de Medeiros Brito [1], Marianna Vieira Sobral [1], Fernando Martins dos Santos Júnior, Maria de Fátima Agra [3], Luciana Scotti [1], Lucas Silva Abreu [2], Marcus Tullius Scotti [1,*], Josean Fechine Tavares [1,*] and Marcelo Sobral da Silva [1]

[1] Federal University of Paraiba, Graduate Program on Natural and Synthetic Bioactive Products (PgPNSB), Health Sciences Center, João Pessoa-PB, Brazil

[2] Fluminense Federal University, Department of Organic Chemistry, Niteroi-RJ, Brazil

[3] Federal University of Paraiba, Center of Biotechnology, João Pessoa-PB, Brazil

*Correspondence: mtscotti@gmail.com (M.T.S.); josean@ltf.ufpb.br (J.F.T.)

Abstract

Belonging to the Euphorbiaceae family, *Jatropha* genus is a promising source for discovering of antitumor compounds. *Jatropha ribifolia* is a traditionally used species in folk medicine in the semi-arid region of Brazil with a few chemical and pharmacological reports. Based on that, the aim of the current work is to isolate, structurally characterize, and assess the cytotoxic activity of isolated compounds through *in vitro* and *in silico* analyses. To achieve these main goals, the underground parts were dried, extracted and purified using classical and instrumental chromatographic techniques, leading to the isolation of 16 compounds. Altogether with HR-ESI-MS, IR, one- and two-dimensional NMR experiments, eight previously unreported diterpenes, named ribifolones A-H, along eight known compounds, were obtained and are herein described. Regarding their activity against melanoma (SK-MEL-28) and colorectal cancer (HCT-116) cell lines, jatrophone was the most potent with IC_{50} of 6.19 μM and 10.09 μM followed by ribifolone that exhibited a moderate cytotoxicity with IC_{50} values of 50.71 μM and 33.39 μM, respectively. Network pharmacology analysis suggests the involvement of PI3K-AKT-mTor pathway in the activity of both compounds, meanwhile molecular docking and dynamics simulations demonstrate the main interactions with key proteins in the pathway and highlighted the estrogen receptor beta (ERβ) as putative target. This work opens new perspectives for the discovery of bioactive compounds found in Euphorbiaceae species, especially from those occurring in Caatinga.

Keywords: terpenoids; target deconvolution; antiproliferative compounds

1. Introduction

Euphorbiaceae is one of the largest genera of flowering plants, among their 340 genera, *Jatropha* includes approximately 175 species [1]. In Brazil, the semi-arid region is home to a diverse range of medicinal species, many of which remain poorly investigated regarding their chemical and pharmacological potential. Among these plants, *J. ribifolia* (Pohl) Bail. stands out as a promising source for the discovery of new bioactive compounds.

Conventionally known as "pinhão-de-purga", *J. ribifolia* latex is used throughout northeastern Brazil due to its antivenom activity. Moreover, its seeds are a source for oil production and are also applied in the veterinary field as purgative [2]. Previous studies report the composition of essential

 doi:10.20944/preprints202603.1635.v1

oil and the isolation of ten compounds from this plant, such as coumarins, an orbitide-type peptide and terpenoids derivatives [3,4], Figure 1. The genus *Jatropha* is an inestimable reservoir of diterpenes with remarkable cytotoxic activity [5]. However, to our knowledge, only two diterpenes were isolated from *J. ribifolia*; jatrophone and 2β-hydroxyjatrophone.

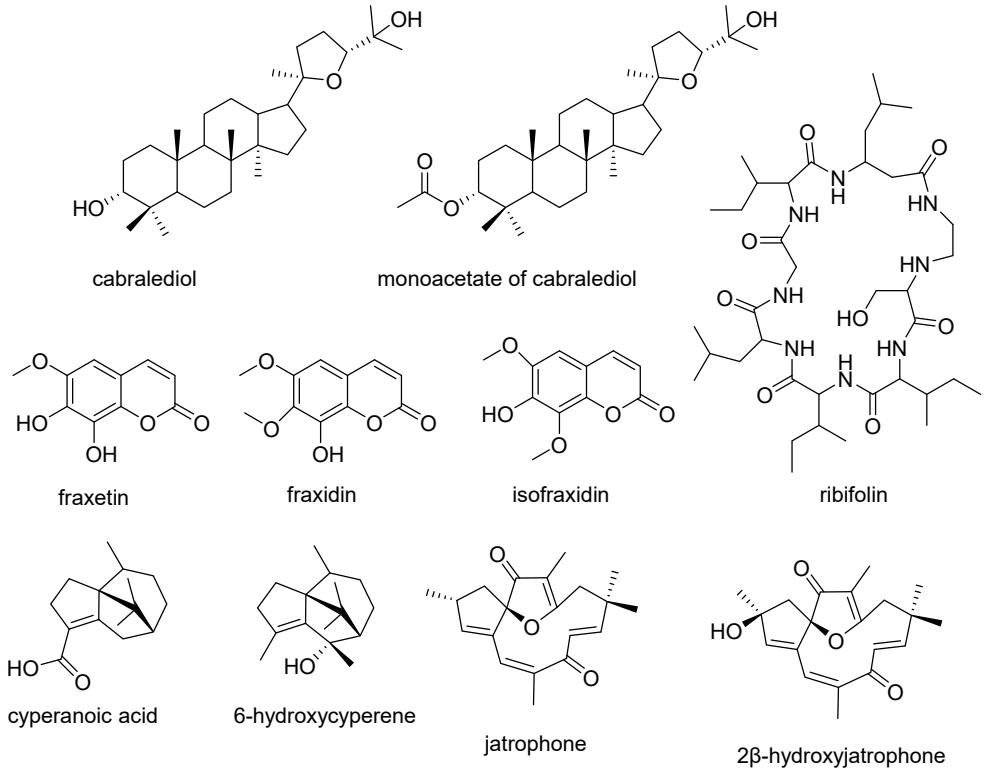

Figure 1. Compounds previously isolated from *J. ribifolia.*

In recent years, the integration of omics sciences with bioinformatics and molecular modeling tools has enabled a more efficient exploration of the chemical space and biological activity associated with natural substances [6]. Based on the principles of polypharmacology, approaches such as network pharmacology have consolidated modern paradigms in the field, allowing not only the rational selection of biological assays to confirm the activity of new chemical entities but also supporting the elucidation of their respective mechanisms of action. These technologies have provided new useful insights for drug repositioning, reinvestigation of classically described natural compounds, and the study of preparations from traditional Chinese medicine [7,8]. Such findings have contributed to highlighting the potential of natural compounds as strategic elements in the development of innovative drugs.

In this context, our research group has been continuously investigating the chemodiversity of the Brazilian Caatinga, unveiling its bioactive potential. Therefore, the main goals of the present work are to isolate, characterize, and evaluate the cytotoxic activity of new macrocyclic diterpenes from *J. ribifolia* through *in vitro* assays and to investigate possible mechanisms of action by *in silico* approaches, including network pharmacology, molecular docking, and molecular dynamics.

2. Results

2.1. Structural Characterization

The hexane extract of *J. ribifolia*'s roots was fractionated by column chromatography and semipreparative HPLC, leading to the isolation of eight unknown diterpenes (**1–8**). Their structures were proposed using 1D and 2D NMR spectroscopy and supported by HR-ESI-MS, and infrared spectroscopy (IR). Besides, eight known compounds were also obtained, 9β,13α-

 doi:10.20944/preprints202603.1635.v1

dihydroxyisabellione (**9**), jatrophone (**10**), 2α and 2β-jatrophone (**11-12**); citlalitrione (**13**), (6S)-patchoulan-4-en-6-ol (**14**), patchoulenone (**15**) and sugeonol (**16**) [4,9–11].

Compound **1** was obtained as a yellowish oil. Its molecular formula was determined as $C_{20}H_{25}O_6$ by HR-ESI-MS at m/z 345.1690 $[M - H_2O + H]^+$ (calcd. for $C_{20}H_{25}O_5$, 345.1697, Δ = 2.0 ppm). The ^{13}C NMR spectrum of compound **1** revealed twenty carbon signals. Among them, signals at δC 212.4 and 202.7 were assigned to ketone and conjugated ketone carbonyl groups, respectively. Additionally, two olefinic carbon signals, two carbinolic carbons, two methylene carbons, and five methyl carbons were observed. In the ^1H NMR spectrum, methyl hydrogen signals appeared at δH 1.83 (d, J = 1.3 Hz), 1.16 (s), 1.13 (s), 1.13 (d, J = 6.7 Hz), and 1.11 (s). Olefinic hydrogen signals were detected at δH 5.63 (bq, J = 1.3 Hz), alongside an oximethinic hydrogen at δH 4.06 (d, J = 12.0 Hz) and 3.34 (s). Analysis of the NMR combined data (Tables 1 and 2) were then compared with literature and allowed the identification of compound **1** as a macrocyclic diterpene analogous to 9β,13α-Dihydroxyisabellione (**9**). Differences between the compounds included the absence of olefinic signals at C-3 and C-4 and the presence of carbinolic signals at δC 75.5 (C-3) and 64.1 (C-4), indicating oxidation at these positions and the formation of an epoxide group.

In the HMBC spectrum, correlations were observed between H-5 and carbons C-3, C-6, C-7, C-15, and C-17; between H-3 and C-1, C-2, C-4, C-15, and C-16; between H3-16 and C-3 and C-1; and between H2-1 and C-3, C-4, and C-14. All chemical shifts of protonated carbons were confirmed by the HSQC spectrum. In the COSY spectrum, correlations were seen between H-3 and H-2, and between H-2 and H3-16, confirming the presence of the epoxide group in this ring (Figure 1).

The NOESY spectra showed cross-peaks between H-3 → H3-16 → H-1β; H-9 → H3-18 → H-11β → H3-20; and H-8 → H3-19, evidencing the relative stereochemistry of compound 1. The compound was named Ribifolone A, a novel natural product.

Compound **2** was obtained as a yellowish oil. Its molecular formula was determined as $C_{20}H_{28}O_6$ by HR-ESI-MS at m/z 347.1857 $[M - H2O + H]^+$ (calcd. for $C_{20}H_{26}O_5$, 347.1853, Δ = -1.3 ppm). The ^1H and ^{13}C NMR analyses of compound **2** revealed twenty carbon signals in the ^{13}C NMR spectrum. Similarly, to observed in Ribifolone A, the compound **2** exhibited in ^{13}C NMR spectrum, the presence of two carbonyl groups at δC 206.8 and 199.8, attributed to ketone and conjugated ketone carbonyl groups, respectively. It also displayed four olefinic carbon signals (as seen in compound **9**) and four carbinolic carbon signals, differentiating it from Ribifolone A. Additionally, in DEPT 135 spectrum, two methylenic carbons and five methyl carbons were identified. In the ^1H NMR spectrum, methyl hydrogen signals were observed at δH 1.06 (d, J = 5.6), 1.98 (s), 1.22 (s), 0.94 (s), and 1.52 (s), with olefinic hydrogens at δH 6.15 (d, J = 2.0) and 6.51 (s), and an oxymethine hydrogen at δH 4.81 (t). The shared similarities between the NMR spectra of Ribifolone A (**1**), 9β,13α-Dihydroxyisabellione (**9**), and compound **2** enabled its identification as a macrocyclic diterpene. Distinct differences included signals at δC 91.1 (C-15) and δC 91.2 (C-12), indicating lactone cleavage and the presence of two carbinolic carbons.

In the HMBC spectrum, correlations were observed between H2-1 and C-2, C-3, C-4, and C-15, between H3-20 and C-12, C-13 and C-14; and between H-8 and C-7, and C-13. In the COSY spectrum, correlations were seen between H-3 and H-2, and H-2 with H3-16 and H2-1, confirming the presence of the double blond in C-3/C-4 (Figure 1). NOESY spectrum showed that H-2→H-1α, H-8 → H3-19, and H-9 → H3-18, demonstrating the relative stereochemistry of compound **2** is similar to compound **1** and **9**. The ^1H and ^{13}C NMR data are shown in Tables 1 and 2. From this evidence, the structure of compound **2** was proposed as a new diterpene, named Ribifolone B.

Compound **3** was obtained as a yellowish oil. Its molecular formula was determined as $C_{20}H_{24}O_4$ by HR-ESI-MS at m/z 351.1572 $[M + Na]^+$ (calcd. for $C_{20}H_{24}NaO_4$, 351.1567, Δ = -1.6 ppm). The ^{13}C NMR spectrum of compound **3** revealed twenty carbon signals, including δC 204.3 and 201.3, corresponding to conjugated ketone carbonyl groups. Additionally, six olefinic carbon signals were observed between δC 112.2 and 185.3, one of which was an oxygenated double bond, and three carbinolic carbons between δC 68.4 and 94.8. Analysis of the NMR data (Tables 1 and 2), along with comparisons to the literature, showed that compound **3** exhibited ^1H and ^{13}C NMR spectra similar to

 doi:10.20944/preprints202603.1635.v1

jatrophone (**10**) and the main difference between them was the absence of olefinic signals at C-3 and C-4 (reported for **10**) and the presence of carbinolic signals at δC 69.1 (C-3) and 67.1 (C-4) in **3**, similar of observed in compound **1**. This indicated oxidation at these positions and the formation of an epoxide group.

In the HMBC spectrum, correlations were observed between H-5 and carbons C-3, C-7, C-15, and C-17; between H-3 and C-1, C-2, C-4, C-15, and C-16; between H3-16 and C-3 and C-1; and between H2-1 and C-3, C-4, and C-14.; H-9 and C-7, C-8, C-18, and C-19; H3-20 and C-12, C-13, C-14. Similarly to compound **1**, in the COSY spectrum, correlations were seen between H-3 and H-2, and between H-2 and H3-16, confirming the presence of the epoxide group in this ring (Figure 1). The NOESY spectra showed cross-peaks between H-3 → H3-16 → H-1β, evidencing the relative stereochemistry of cyclopentane in **3**.

Compound **4** was obtained as a yellowish oil. Its molecular formula was determined as $C_{20}H_{24}O_4$ by HR-ESI-MS at m/z 311.1632 $[M - H_2O + H]^+$ (calcd. for $C_{20}H_{23}O_3$, 311.1642, Δ = 3.3 ppm). Compound **4** featured twenty carbon signals in its ^{13}C NMR spectrum. It was observed the presence of two carbonyl signals in δC 204.4 and 202.3 attributed to conjugated ketone carbonyl groups, eight olefinic carbons, two carbinolic carbons (δC 93.9 and 97.7), two methylene carbons, and five methyl carbons. Likewise compounds **3** and **10**, the presence of one oxygenated double bond in δC 185.6, indicated structural similarities to jatrophone. In the ^1H NMR spectrum, five methyl hydrogen signals were observed at δH 1.95 (d, J = 1.3), 1.73 (s), 1.64(s), 1.33 (s), and 1.21 (s). Olefinic hydrogens were identified at δH 6.11 (bs), 6.10 (s), 6.00 (d, J = 13.2 Hz), and 6.5 (d, J = 13.2 Hz). The presence of three methyl groups linked to double bonds and the absence of the characteristic signs of the epoxide group present in compound **3** indicates the presence of a double bond between carbons C-2 and C-3. Furthermore, the signal at δC 93.9, which is not present in the DEPT 135 spectrum, indicates the presence of a hydroxyl group at C-4.

In the HMBC spectrum, correlations were observed between H-5 and carbons C-3, C-6 and C-15; between H-3 and C-1, C-2, C-4, C-15, and C-16; between H3-16 and C-1, C-3; between H2-1 and C-2, C-3, C-4, C-14, and C-16; All chemical shifts of protonated carbons were confirmed by the HSQC spectrum. In the COSY spectrum, correlations were observed between olefinic hydrogens H-8 and H-9 and H-5 and H-17, confirming the presence of two other double bonds, one tri-substituted and the other tetra-substituted (Figure 1). From this evidence, the structure of compound 4 was proposed as a new diterpene, named Ribifolone D.

Compound **5** was obtained as a yellowish oil. Its molecular formula was determined as $C_{20}H_{22}O_3$ by HR-ESI-MS at m/z 311.1637 $[M+H]^+$ (calcd. for $C_{20}H_{23}O_3$, 311.1642, Δ = 1.5 ppm). Compound **5** exhibited twenty carbon signals in its ^{13}C NMR spectrum, including δC 203.2 and 201.9, corresponding to two conjugated ketone carbonyl groups. Additionally, ten olefinic carbon signals and four methyl carbon signals were observed. The ^1H NMR spectrum displayed four methyl hydrogen signals at δH 1.98 (d, J = 0.8), 1.77 (s), 1.36 (s) and 1.23 (s). As observed previously, the presence of an oxygenated double bond at δC 185.3 indicates the presence of a jatrophone-type structure, similar to compounds **3**, **4**, and **10**. Differences between compound **5** and jatrophone (**10**) were indicated by signals at δC 148.9 (C-2) and δC 109.6 (C-16), suggesting the presence of an exocyclic double bond. This was supported by hydrogen signals at δH 5.10 (bs) and 5.25 (bs).

In the HMBC spectrum, correlations were observed between H-3 and carbons C-2, C-4 and C-15; between H3-16 and C-1, C-3; between H-9 and C-7, C-11 and C-19. In the COSY spectrum, there were observed correlations between H-8 and H-9, H-5 and H3-17 and H3-16 and H2-1. From this evidence, the structure of compound 5 was proposed as a new diterpene, named Ribifolone E.

Compound **6** was obtained as a yellowish oil. Its molecular formula was determined as $C_{20}H_{26}O_4$ by HR-ESI-MS at m/z 331.1903 $[M + H]^+$ (calcd. for $C_{20}H_{27}O_4$, 331.1904, Δ = 0.1 ppm). Compound 6 displayed twenty carbon signals in its ^{13}C NMR spectrum, including three carbonyl signals at δC 214.7, 211.5, and 211.2, corresponding to two ketones and one conjugated ketone. Additionally, olefinic carbon signals were detected at δC 139.1 and 129.1. These signals suggest a different skeletal structure compared to previous compounds. Analysis of the spectroscopic data, supplemented by a

 doi:10.20944/preprints202603.1635.v1

comparison with the literature, revealed that compound 4 closely resembled citlalitrione (**13**), with differences in the signals for carbons C-3, C-4, and H3-16 (Table 2). Yang et al., 2003, synthesized Citlalitrione with a β-epoxy group (δC 72.5 and 67.8), similarly the chemical shifts observed compound 13, and your isomer with an α-epoxy group (δC 65.2 and 66.6), like the chemical shifts observed for compound 6. Thus, the stereochemical inversions of the epoxide between C-3 and C-4, as well as the methyl group Me-16, were proposed.

The NOESY spectrum showing crossed peaks between H-3→H3-16, H-15→H3-20 confirmed that the hydrogens are in the same plane and crossed peaks between H-9 and methyls 17, 18, and 19 show that it is not possible to establish the orientation of H-9. The compound was named Ribifolone F, a novel macrocyclic diterpene.

Compound **7** was obtained as a yellowish oil. Its molecular formula was determined as $C_{20}H_{26}O_4$ by HR-ESI-MS at m/z 313.1798 $[M - H_2O + H]^+$ (calcd. for $C_{20}H_{25}O_3$, 313.1798, Δ = 1.4 ppm). Compound **7** displayed twenty carbon signals in its 13C NMR spectrum, including three carbonyl signals at δC 214.7, 211.3, and 209.1, corresponding to two ketones and one conjugated ketone. These findings suggested a resemblance to compounds **6** and **13**, a cyclojatrophane. The distinction between compound **7** and the previously identified substance was observed in four olefinic carbon signals at δC 125.2 (C-5), 143.6 (C-6), 143.0 (C-4), and 139.7 (C-5), the absence of a carbinolic hydrogen signal at δH 3.4 (C-15), and differences in the chemical shift of the oxymethine proton from δH 3.16 (s) to δH 4.27 (d, J = 4.0). The shift in the C-3 carbon signal from δC 65.8 to δC 86.9 further supported this distinction.

In the HMBC spectrum, correlations were observed between H3-16 and C-1, C-3; between H3-17 and C-5, C-6, C-7; between H3-20 and C-9, C-12, C-13, C-14. (Figure 1). The NOESY spectrum showed crossed peaks between H-9→H3-19, H3-20→H-11→H3-18, as also observed in compounds **6** and **13**. From this evidence, the structure of compound **7** was proposed as a new diterpene, named Ribifolone G.

Compound **8** was obtained as a yellowish oil. Its molecular formula was determined as $C_{20}H_{26}O_5$ by HR-ESI-MS at m/z 369.1672 $[M + Na]^+$ (calcd. for $C_{20}H_{26}NaO_5$, 369.1672, Δ = 0.1 ppm). The ^{13}C NMR spectrum of compound 8 revealed twenty carbon signals. Among them, two signals at δC 208.5 and 203.4 were assigned to ketone and conjugated ketone carbonyl groups, respectively. Additionally, one olefinic carbon signal, one carbinolic carbons, two methylene carbons, and five methyl carbons were observed.

In the ^1H NMR spectrum, methyl hydrogen signals appeared at δH 1.83 (d, J = 1.3 Hz), 1.16 (s), 1.13 (s), 1.13 (d, J = 6.7 Hz), and 1.11 (s). Olefinic hydrogen signals were detected at δH 5.63 (ql, J = 1.3 Hz), alongside oximethinic hydrogens at δH 4.06 (d, J = 12.0 Hz) and 3.34 (s). Analysis of the NMR data (Tables 1 and 2),

In the HMBC spectrum, key correlations were observed between olefinic proton H-5 and carbons C-3, C-7, C-15, CH3-17. Additionally, the correlations observed from the the methyl groups were also important to structural elucidation, among them CH3-16 and C-1, C-2 and C-3, CH3-17 with C-5, C6 and C-7, between CH3-18 with C-9, C10 and C-11 and similar correlations of CH3-20 and C-12, C-13 and C14. The chemical shifts attributed to protonated carbons were confirmed by the HSQC spectrum.

In the COSY spectrum, correlations were seen between CH3-16 and H-2, H-2 and H-3, confirming the presence of a hydroxyl group in C-3. Additionally, the correlations between H-8 and H-9, H-9 and H-11 suports the presence of a cuclopropane ring in the structure. The NOESY spectra showed cross-peaks between H-3 → H3-16 → H-1β; H-9 → H3-18 → H-11β → H3-20; and H-8 → H3-19, evidencing the relative stereochemistry of compound 1.

Based on the chemical shifts, comparison with published literature and the observed correlations, the obtained data indicated structural similarities between compound **8** and multifidanol, a lathyrane diterpene previously isolated from *J. multifida* [12] . Differing from this compound, **8** exhibits the additional signal at 208.5 attributed to C-7, the chemical shifts attributed to CH_3-20, C-12, and C-15 confirmed the presence of a substituted 2-oxolane ring, as previously

 doi:10.20944/preprints202603.1635.v1

observed in ribifolones C, D, and E and in other jatrophane-type diterpenes isolated from *J. ribifolia*. These structural features result in a rare combination of motifs within the molecule. Considering this set of evidence, the structure of compound 8 was proposed as a new diterpene, named Ribifolone H.

Among the eight new diterpenes described, five of them are jatrophanes, one belongs to the lathyrane class, and the last two are rare cyclojatrophane derivatives. Only two other 9,13-cyclojatrophane compounds have been previously reported in the *Jatropha* genus, namely citlalitrione and jatrophatrione [38,39]. These findings highlight the remarkable chemodiversity contained in plant species from the Brazilian semi-arid region. Tables 1 and 2 summarize the chemical shifts of ^{1}H and ^{13}C NMR of compounds **1-8**. Figure 1 depicts the correlations observed in HMBC and NOESY spectra.

Table 1. ^{1}H NMR data at 400 MHz, in $CDCl_3$, for Ribifolones A-H (1-8), *J* in Hz.

	1	**2**	**3**	**4**	**5**	**6**	**7**	**8**
Position	δ_H	δ_H	δ_H	δ_H	δ_H	δ_H	δ_H	δ_H
1α	2.22 dd (14.4; 8.4)	2.43 m	1.67 m	2.6 d (12)	2.99 dt (1.6)	1.24 d (13.3)	2.11 m	1.9 m
1β	1.89 d (14.4)	2.11 d (4.4)	2.04 dd (14.3; 8.3)	2.2 d (12)	2.83 m	1.64-1.54 m	2.71 m	2.1 m
2	2.38 m	2.99 m	2.48 dd	-	-	2.12-2.06 m	2.12-2.08 m	2.32 m
3	3.34 s	6.15 d (2.0)	3.20 m	6.10 s	6.6 s	3.16 sl	4.27 d (4.0)	4.05 d (3,6)
4	-	-	-	-	-	-	-	
5	5.63 ql (1.3)	6.51 s	5.74 dd (3.22. 1.6)	6.11 bs	6.3 bs	5.24 ql (1.6)	5.99 s	5.7 sl
6	-	-	-	-	-	-	-	
7	-	-	-	-	-	-	-	
8	3.82 d (11.3)	3.31 d (1.6)	6.23 d (16.5)	6.0 d (13.2)	6.01 d (12.0)	2.56-2.50 m	2.78 d 2.81 d (1.6)	2.83 dd 2.75 dd
9	4.05 d (11.3)	4.81 t	6.41 d (16.5)	6.5 d (13.2)	6.54 d (12.0)	2.84 dd (10.0; 1.7)	2.59 d (2.0)	1.73 m
10	-	-	-	-	-	-	-	
11α	2.13 d (15.3)	2.30 dd (1.6; 1.6)	2.48 dd (0.8; 0.8)	2.7 d (12.0)	2.80 m	2.43 d (16.0)	2.49 d (10.8)	2.0 d (12)
11β	1.86 d (15.3)	2.60 d (13.6)	2.86 d (14.8)	2.4 d (12.0)	2.50 m	2.24 d (16.0)	2.23 d (12.8)	
12	-	-	-	-	-	-	-	-
13	-	-	-	-	-	-	-	-
14	-	-	-	-	-	-	-	-
15	-	-	-	-	-	3.41 dd (10.0; 7.5)	-	-
16	1.12 d (6.6)	1.06 d (5.6)	1.20 d (7.6)	1.65 s	5.10 bt (1.6) 5.25 bt (1.6)	1.05 d (7.5)	1.14 d (5.2)	1.1 sl
17	1.83 d (1.3)	1.98 d (1.5)	1.83 d (1.5)	1.95 d (1.3)	1.98 d (0.8)	1.90 d (1.6)	1.95 d (1.5)	1.30 s
18	1.11 s	0.94 s	1.22 s	1.21 s	1.23 s	1.21 s	1.28s	1.41 s
19	1.13 s	1.22 s	1.41 s	1.33 s	1.36 s	0.84 s	0.88s	1.39 s
20	1.16 s	1.52 s	1.70 d (0.7)	1.73 s	1.77 s	1.34 s	1.32 s	1,78 s

Table 2. ^{13}C NMR data at 100 MHz, in $CDCl_3$, for Ribifolones A-H (1-8), δ_C in ppm.

	1	**2**	**3**	**4**	**5**	**6**	**7**	**8**
Position	δ_C	δ_C	δ_C	δ_C	δ_C	δ_C	δ_C	δ_C
1	44.4	46.0	37.6	41.5	37.1	33.6	41.6	44.1

 doi:10.20944/preprints202603.1635.v1

2	31.0	37.0	33.2	139.0	148.9	34.9	43.0	36.4
3	75.6	148.9	69.2	136.2	135.9	65.8	86.9	83.1
4	64.0	140.8	68.4	93.9	142.1	66.8	143.0	138.2
5	131.4	127.3	122.9	136.3	137.2	129.1	125.2	132.2
6	143.5	137.7	142.3	143.9	142.2	139.1	143.6	77.0
7	202.7	199.8	201.3	202.3	201.9	211.2	209.1	208.5
8	66.5	66.9	129.7	128.7	128.3	38.8	38.9	33.6
9	79.9	80.8	158.3	158.6	157.7	49.2	51.1	31.4
10	37.2	37.8	36.7	40.9	40.8	37.6	37.4	29.4
11	43.2	48.9	41.7	43.3	43.2	55.2	55.4	27.6
12	77.6	91.1	185.3	185.6	185.3	214.7	214.7	189.0
13	89.4	88.0	112.2	113.4	113.1	64.0	64.2	109.5
14	212.4	206.8	204.4	204.4	203.2	211.5	211.3	203.4
15	87.0	91.0	94.8	97.7	98.5	45.6	139.7	91.1
16	16.5	20.4	17.2	24.2	109.6	14.9	18.2	14.3
17	22.1	20.7	21.4	13.3	13.1	21.2	19.2	29.4
18	27.6	25.3	30.8	30.4	30.3	27.6	27.3	28.8
19	22.3	28.0	27.2	26.5	26.3	23.6	23.6	15.4
20	14.0	17.3	6.1	7.3	7.2	14.2	14.5	5.8

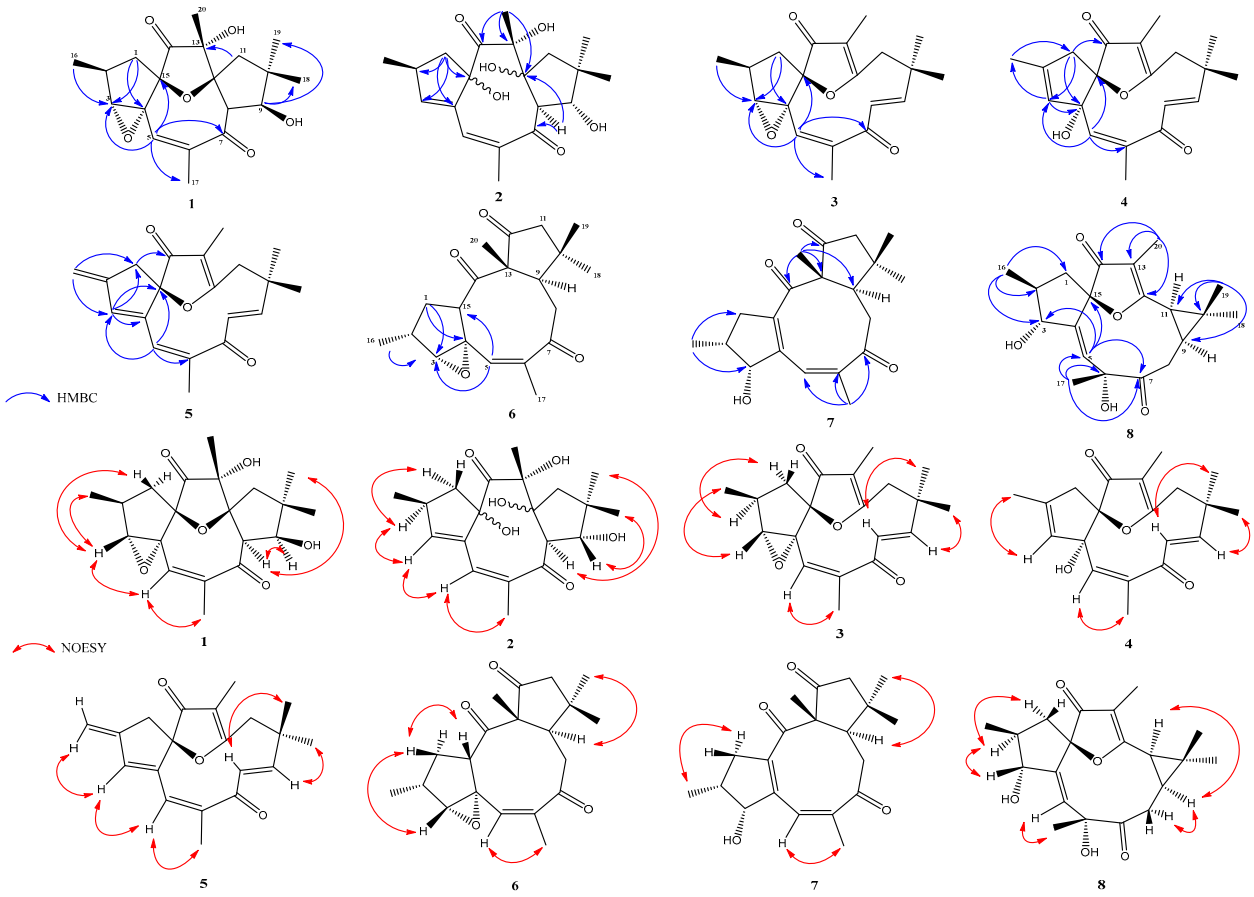

Figure 2. Key correlations of HMBC and NOESY of ribifolones 1-8.

2.2. Biological Assay

After structural elucidation, ribifolones A–H were evaluated against two human tumor cell lines. The selected SK-MEL-28 (melanoma) and HCT-116 (colorectal cancer) were subjected to the MTT reduction assay after 72 h of treatment with the compounds. Table 3 presents the corresponding results.

 doi:10.20944/preprints202603.1635.v1

Table 3. Cytotoxicity of ribifolones A-H in micromolar (μM), using the MTT reduction assay after 72 hours of treatment. The data is presented as the half-maximal (50%) inhibitory concentration (IC_{50}) values as the mean ± SEM (three independent experiments in triplicate), calculated by nonlinear regression analysis using concentration–response curves.

Compounds	IC_{50} (μM)		
	Cell lines		
	SK-MEL-28	HCT-116	HEK-293
ribifolone A	32.25 ± 2.41	> 100.0	> 100.0
ribifolone B	> 100.0	> 100.0	-
ribifolone C	50.71 ± 3.80	33.39 ± 1.98	> 100.0
ribifolone D	95.64 ± 1.51	75.35 ± 4.82	> 100.0
ribifolone E	> 100.0	> 100.0	-
ribifolone F	> 100.0	> 100.0	-
ribifolone G	> 100.0	> 100.0	-
ribifolone H	> 100.0	> 100.0	-
jatrophone	6.19 ± 0.96	10.09 ± 0.61	20.28 ± 0.98

In the set of the new compounds tested, only three of them exhibited cytotoxicity. Demonstrating a moderate activity, ribifolone C achieved IC_{50} values of 50.71 and 33.39 μM against melanoma and colorectal cancer cells, respectively. Ribifolone A, inhibited cell viability only against melanoma (IC_{50} = 32.25 μM). Meanwhile, ribifolone D acted on both tumor lines, although with lower potency (IC_{50} = 95.64 and 75.35 μM) than ribifolone C. Ribifolones B and E–H, were considered as inactive, Table 3.

Known by its high cytotoxicity against different cancer cell types, jatrophone is the major compound found in the roots of *J. ribifolia* [4,13]. To compare how structure modifications could reflect over the biological activity, jatrophone was also tested and displayed the strongest activity among the series (IC_{50} = 6.19 μM in SK-MEL-28 and IC_{50} = 10.09 μM for HCT-116).

The evaluation of the selectivity index (SI) is a crucial step in the early stages of drug discovery. However, many previously published studies report the bioactivity of medicinal plants and their isolated compounds without providing SI data, which represents a limitation for further pharmacological development [14]. In this context, compounds that exhibited cytotoxic activity were further evaluated in HEK-293 cells, a non-tumoral human embryonic kidney cell line. Regarding selectivity, ribifolones A and C–D showed IC_{50} values > 100 μM, indicating low cytotoxicity toward normal cells, Table 3. Consequently, SI values were calculated for jatrophone, which was 3.28-fold more selective for SK-MEL-28 cells and 2.01-fold more selective for HCT-116 cells.

Literature reports many diterpenes as remarkable antitumor compounds, among them lathyrane and jatrophane typically occur in *Jatropha* species [15]. In the current study, only the jatrophane-type derivatives exhibited cytotoxic activity. Compared to jatrophone, the results imply that differences in oxidation patterns such as presence of epoxide between C-2 and C-3, hydroxyl groups in C-4 and C-9 constitute a key factor in modulating the bioactivity. Furthermore, structural changes such as lactone cleavage, variations in the size of macrocyclic ring and substitutions in the double bonds may have contributed to the weaker antitumor activity of ribifolones against the selected cell lines.

Despite some previous reports demonstrating that the acetoxy group at C-9, benzoyl moiety occupying position 3 and propyl group at C-8 decreases cytotoxicity of some jatrophane diterpenes, many aspects about this topic remain unclear, especially due to diversity of tumor lineages presented in each work ([16,17]. Based on that, complementary studies designed with a larger number of analogs and well-defined cell lines are required to obtain suitable data to develop QSAR models.

Regarding their mechanisms of action, despite being recognized as promising scaffolds, macrocyclic diterpenes from *Jatropha* remain largely unexplored [18]. In this context, the use of modern approaches such as network pharmacology and molecular modeling, including docking and dynamics, has become increasingly common in the study of natural products. The combination of

 doi:10.20944/preprints202603.1635.v1

these methods also assists in identifying pharmacophoric groups and other key properties relevant to the development of pharmacological studies, whether *in vitro* or *in vivo* models.

2.3. Pharmacological Network and Molecular Modeling

To elucidate the potential mechanisms underlying the effects of the active compounds, a combination of *in silico* approaches was employed. Based on the activity of ribifolone C and jatrophone against both cell lines, a network pharmacology workflow was applied to colorectal and melanoma cancers to explore their putative molecular targets. In this context, analyses performed using the PharmMapper and AiA platforms identified 271 proteins as potential targets for the compounds, whereas GeneCards retrieved 3,485 and 2,290 genes associated with colorectal and melanoma cancers, respectively. The intersection analysis identified proteins encoded by disease-associated genes that overlapped with the predicted protein targets, yielding 118 candidates for colorectal cancer and 80 for melanoma.

For both cancer types, the resulting networks exhibited high interconnectivity, with average node degrees of 8.73 for colorectal cancer and 8.25 for melanoma, indicating a complex pattern of molecular interactions. Several hub genes present degrees equal to or greater than 15, suggesting that these nodes may represent key points of functional convergence within cancer-related pathways. In network pharmacology, highly connected nodes are often considered topologically influential, as their modulation may affect multiple interconnected biological processes rather than a single signaling route. Accordingly, the application of a degree threshold of 17 allowed the prioritization of the most interconnected targets, highlighting a subset of proteins that may collectively contribute to the biological effects observed for ribifolone C and jatrophone. This network topology supports the hypothesis that its activity is mediated through a multi-target mechanism, as illustrated in Figure 3.

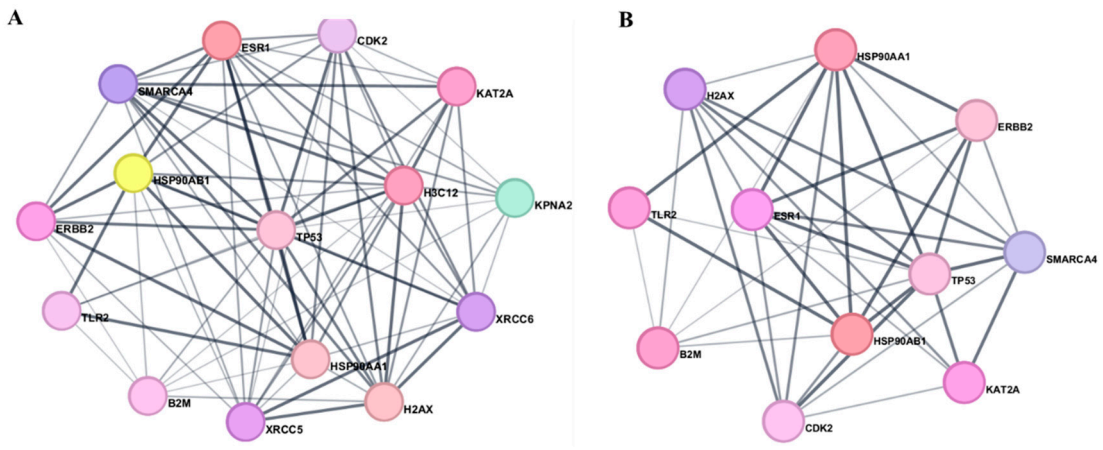

Figure 3. Network pharmacology interaction networks of ribifolone C and jatrophone in colorectal cancer (A) and melanoma (B), emphasizing highly connected hub proteins. Node colors were applied exclusively for visual differentiation.

As shown in Figure 4, KEGG enrichment analysis indicated that the PI3K–Akt–mTOR signaling pathway presented the highest GeneRate value in both colorectal and melanoma networks. The Kyoto Encyclopedia of Genes and Genomes (KEGG) is a curated resource that links genes and proteins to canonical biological pathways, enabling functional interpretation of disease-associated gene sets. In this context, the observed enrichment suggests that a considerable fraction of genes associated with these cancers, whose encoded proteins overlap with the predicted targets of ribifolone C and jatrophone, converge on the PI3K–Akt–mTOR axis. Notably, this pathway is frequently deregulated in cancer and is known to regulate essential cellular processes, including proliferation, survival, growth, and metabolism [19,20].

 doi:10.20944/preprints202603.1635.v1

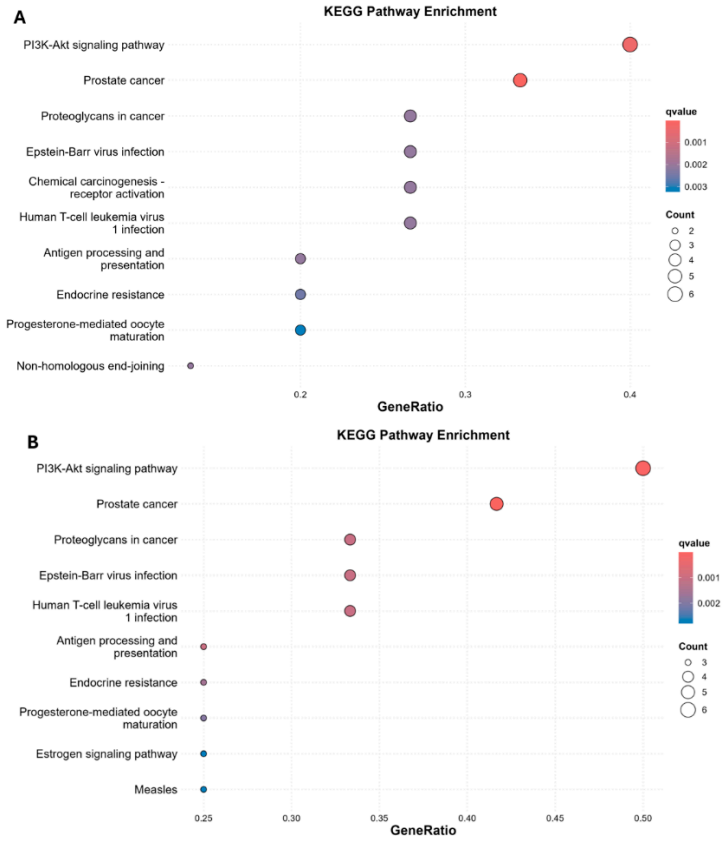

Figure 4. KEGG pathway enrichment analysis of colorectal (A) and melanoma (B) cancer-associated genes overlapping with the predicted targets. The x-axis shows the GeneRatio, circle size represents *Count*, and color indicates the q-value, with red corresponding to higher enrichment significance.

Given the prominence of the PI3K–Akt–mTOR signaling pathway as a potential component of the mechanism of action associated with the selected compounds, molecular docking simulations were performed focusing on key proteins within this pathway, the results are summarized in Table 4. Docking scores were used to estimate the binding energies of the complexes formed between the ligands and the selected targets, with more negative values indicating greater complex stability [21]. The ligand efficiency (LE) was calculated as the ratio of docking score to the number of heavy atoms, as previously mentioned.

Table 4. Docking results for target proteins comparing ribifolone C, jatrophone, and reference ligands displaying Moldock score, ligand efficiency (LE), and RMSD values.

Protein	Ligand	Moldock Score	LE	RMSD (Å)
ERα	ribifolone C	-99.6025	4.15	
	jatrophone	-99.9278	4.34	
	Compound 15	-176.836	5.20	0.152
ERβ	ribifolone C	-103.407	4.31	
	jatrophone	-106.904	4.65	
	WAY-697	-113.646	3.67	0.137
HER2	ribifolone C	-109.498	4.56	
	jatrophone	-109.166	4.75	
	SYR127063	-211.971	6.23	0.206
HSP90α	ribifolone C	-93.2953	3.89	

 doi:10.20944/preprints202603.1635.v1

	jatrophone	-92.7489	4.03	
	PU3	-133.74	4.46	0.226
PI3Kγ	ribifolone C	-131.08	2.49	
	jatrophone	-133.74	2.36	
	PF-04979064	-133.74	3.86	0.337

Regarding the interaction profiles between the diterpenes and the target receptor, docking analysis indicated that the reference agonist WAY-697 achieved the most favorable binding score (−113.65) against ERβ when compared with ribifolone C (−103.41) and jatrophone (−106.90). Nevertheless, ligand efficiency analysis revealed that WAY-697 exhibited the lowest LE value (3.67), whereas jatrophone (4.65) and ribifolone C (4.31) displayed higher efficiencies. WAY-697 was employed as the reference ligand, as it is a potent and selective ERβ agonist with an IC_{50} value of 1.9 nM.

Both diterpenes displayed comparable binding patterns, dominated by hydrophobic interactions with residues Met295, Leu298, Leu301, Ala302, Phe356, His475, and Leu476 (Figure 5). However, ribifolone C formed a greater number of unfavorable contacts (Phe356) compared to jatrophone (Met336), which may account for the differences observed in docking scores and LE values. WAY-697 interacted with ERβ through hydrophobic contacts involving Leu298, Ala302, and Phe356, and established three hydrogen bonds: one conventional with Leu476, and two additional ones with Glu305 and Arg346, Figure SX. The agonist shared four key interactions with ribifolone C and jatrophone (Ala302, Leu339, and Leu476), which may represent critical residues associated with agonistic activity. Detailed information on the interaction profiles of ribifolone C, jatrophone, and the other selected targets is provided in the Supplementary Material.

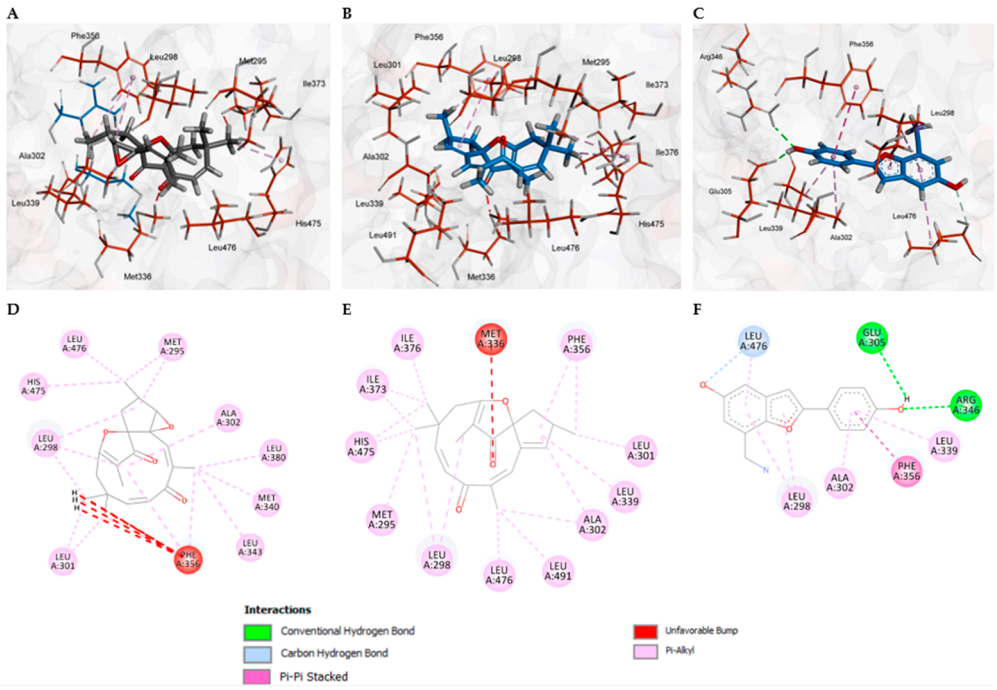

Figure 5. Amino acid interactions formed between ribifolone C (A and D), Jatrophone (B and E), and the reference ligand WAY-697 (C and F) against ERβ.

Estrogen receptors (ERs) are nuclear receptors frequently associated with the pathophysiology of cancer [22]. These receptors exist in two main isoforms, ER*α* and ERβ. ER*α* is commonly linked to tumor cell proliferation and survival, whereas ERβ generally acts as a tumor suppressor, downregulating processes such as proliferation, differentiation, angiogenesis, and immune invasion. Although melanoma and colorectal cancer are not classically described as hormone-dependent

 doi:10.20944/preprints202603.1635.v1

malignancies, accumulating evidence suggests that their progression may be influenced by estrogen receptor expression [23–25].

In colorectal cancer, ER expression exhibits distinct regulatory patterns. ERβ is frequently downregulated, a feature that may contribute to increased cancer cell proliferation. Conversely, ERα, which is typically expressed at low levels in healthy colon tissue, tends to be upregulated, particularly through activation of the PI3K/Akt signaling pathway. In melanoma, the role of ERα remains less clearly defined, whereas ERβ predominates and exerts tumor-suppressive effects by inhibiting PI3K/Akt signaling, thereby restraining cell proliferation and promoting apoptosis [26].

Given that molecular docking analyses indicated more favorable binding scores for ribifolone C and jatrophone toward ERβ when compared with the reference agonist WAY-697, molecular dynamics (MD) simulations were subsequently performed to assess the stability and conformational behavior of the resulting complexes over time. For this purpose, root mean square deviation (RMSD), root mean square fluctuation (RMSF), and interaction energy values were calculated for ERβ complexes with ribifolone C, jatrophone, and WAY-697. The results of the MD simulations are summarized in Table 5.

Table 5. Interaction energy, RMSD, and total drift values obtained from molecular dynamics simulations for ERβ complexes with ribifolone C, jatrophone, and WAY-697.

Molecule	Energy	Average	RMSD (Å)	Total-Drift
Ribifolone C	Coulombic	-68.839	30.630	-50.900
	Lennard-Jones	-77.920	16.805	-19.054
Jatrophone	Coulombic	-25.577	19.671	18.438
	Lennard-Jones	-78.050	18.327	9.609
WAY-697	Coulombic	-158.979	39.815	-58.408
	Lennard-Jones	-51.151	20.575	-43.673

The results of the MD simulations demonstrates that WAY-697 exhibits the most favorable total interaction energy (−210.13 kJ·mol^{-1}), primarily driven by electrostatic contributions calculated through Coulombic forces. In contrast, for ribifolone C total interaction energy (−146.76 kJ·mol^{-1}) hydrophobic interactions represents the major stabilizing contribution, followed by electrostatic forces. A similar interaction pattern was observed for jatrophone, although with a less favorable total energy (−103.82 kJ·mol^{-1}). This energetic profile is consistent with the lipophilic nature of the diterpenes and the predominantly hydrophobic binding environment of ERβ. Rather than indicating unexpected interaction features, these results support the docking, confirming that the predicted binding modes are energetically sustained over the simulation time.

In this context, the complementary outcomes of molecular dynamics and docking normalization analyses indicate that WAY-697 exhibits greater dynamic stability, whereas ribifolone C and jatrophone display higher ligand efficiency. As illustrated in Figure 6, the RMSD and RMSF profiles reflect these distinct dynamic behaviors of the ERβ complexes, supporting an interpretation in which the diterpenes present efficient binding characteristics, while the co-crystallized ligand maintains enhanced structural stability within the ERβ binding site.

 doi:10.20944/preprints202603.1635.v1

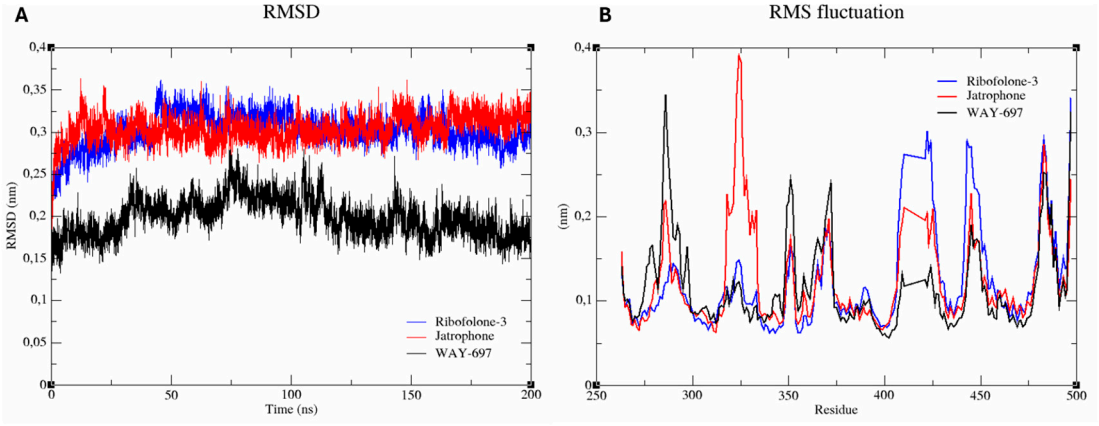

Figure 6. Molecular dynamics simulation analysis of ERβ complexes with ribifolone C, jatrophone, and the reference ligand WAY-697. Interaction energy plots (A) Root mean square deviation (RMSD) and (B) root mean square fluctuation (RMSF) profiles of the protein–ligand complexes over the simulation time.

The results obtained from network pharmacology and molecular modeling analyses suggest the involvement of the PI3K–AKT–mTOR signaling pathway in the activity of ribifolone C and jatrophone, with estrogen receptors, particularly ERβ, emerging as potential targets for these compounds. Such receptors play a key role in the pharmacotherapy of different types of cancer, including breast and prostate cancer. Previous studies have demonstrated the cytotoxic activity of jatrophone against MCF-7 cells (IC_{50} = 1.8 μM), a resistant breast cancer cell line [4]. Regarding its mechanism of action in breast cancer, jatrophone has been shown to act by targeting the PI3K/AKT/NF-κB and Wnt/β-catenin signaling pathways [21,22]. Considering ribifolones as structurally related compounds to jatrophone, the *in silico* predictions discussed herein are consistent with the cytotoxic activity reported for jatrophane-type diterpenes. However, experimental validation is still required, as the complexity inherent to biological systems makes their precise *in silico* si-mulation challenging; therefore, validation using experimental data is essential to determine both the predictive ability and applicability of a computational model [27,28].

3. Materials and Methods

3.1. General Experimental Procedures

Isolation and purification were performed by different chromatographic methods, including column chromatography (CC) and thin-layer chromatography (TLC). Silica gel (Silicycle, particle size of 0.040–0.063 mm) was used for CC. Commercial silica gel (Whatman) plates were used in TLC in layers with a thickness of 0.25 mm on an aluminum support (20 × 20 cm). The spots in TLC were analyzed by using ultraviolet radiation at wavelengths of 254 and 366 nm (Boitton brand apparatus). Additionally, a high-performance liquid chromatography (HPLC) Shimadzu Proeminence apparatus coupled with photodiode array detector (PDA) was also used, separations were carried out in an analytical C18 (YMC; 250 mm × 4.6 mm × 5 μm) and preparative C18 (YMC; 250 mm × 21.2 mm × 5 μm) columns. The mobile phases were composed of ultrapure water (A) (Milli-Q®, Massachusetts, United States of America) and Acetonitrile HPLC grade (B) (Supelco, Sigma-Aldrich.

The IR spectra was recorded on a Fourier transform infrared spectrophotometer (Shimadzu IRSpirit-T) using the QATR-S accessory. The 1D and 2D NMR experiments were conducted using two NMR spectrometers (Bruker Ascend 400 and 100 MHz for 1H and 13C and Bruker AvanceNeo 500 and 125 MHz). The 1H and 13C NMR chemical shifts were referenced to the solvent peaks for residual internal CDCl3. A mass spectrometer (MicroTOF II, Bruker Daltonics, Billerica, MA, USA) with an electrospray ion source (ESI) was used to perform ESI-TOF-MS analysis.

 doi:10.20944/preprints202603.1635.v1

3.2. Plant Material

The botanical material of the species was collected in the city of Serra Branca-PB in March 2016 and identified by Prof. Maria de Fátima Agra. The voucher specimen was deposited at the Lauro Pires Xavier Herbarium (UFPB) under voucher number 123491. The access registration in the National System for the Management of Genetic Heritage and Associated Traditional Knowledge (SISGEN) was obtained under number A22E9B0.

3.3. Extraction and Isolation

The underground parts were dried at room temperature for 72 hours, yielding 245.0 g. The botanical material was then ground and macerated with hexane (3 L) for 7 days, with this process repeated three times. The extract solutions were filtered and concentrated under reduced pressure at 40 °C, resulting in 2.53 g of hexane extract from the roots (JRRHx). After that the process of extraction was repeated with methanol, resulting in roots methanolic extract.

Initially, 2.45 g of JRRHx was subjected to column chromatography (CC) using silica gel 60 (0.063–0.2 mm) as the stationary phase. The extract was eluted with hexane, ethyl acetate, or binary mixtures in a gradient of increasing polarity; 150 mL were collected for each fraction, and the column was completed with pure methanol, yielding 33 fractions. The fractions were then analyzed by TLC, using plates eluted with a hexane and ethyl acetate gradient and visualized under UV light at 296 and 364 nm. Subsequently, the fractions were analyzed by analytical-scale HPLC with exploratory gradients ranging from 50% to 100% acetonitrile (ACN) and water over 60 minutes. The fractions were also subjected to 1H NMR analysis in CDCl3. Fraction FR09 (700 mg) showed a single band on TLC and was directly analyzed by NMR. Meanwhile, the remaining fractions were grouped were analyzed HPLC and 1H NMR to identify their similarity, resulting in the following sets: FR3-5 (135.0 mg), FR11-13 (352 mg), FR-15-16 (50 mg) and FR20-22 (95 mg).

All mentioned samples were subsequently subjected to exploratory analyses on analytical HPLC and further fractionated on semipreparative-scale HPLC after method optimization (data not shown). The chromatographic conditions used for isolation in each sample are provided as follows, for FR3-5 the chromatography run begins with 0.0 - 40.0 min (70 - 1000% of B); 40.0 - 60.0 min (100 - 100% of B); 60.0 - 65.0 min (100 - 70% of B), volume injection of 100 µL and flow of 3 mL/min. For fraction encoded as FR11-13 a gradient ranging from 0.0-75.0 min (35-100% of B), 75.0 - 85.0 min (100 - 100% of B); 85.0 - 90.0 min (100 - 35% of B). In FR-15-16 the system was settled as 0.0-40.0 min (10-80% of B), 40.0 - 45.0 min (80 - 100% of B); 45.0 - 60.0 min (100 - 100% of B), 60.0 - 65.0 min (100 - 100% of B). For fraction FR20-22 the elution was carried out from 0.0 - 40.0 min (35% of B), 40.0 - 45.0 min (35 - 45% of B); 45.0 - 75.0 min (45% of B), 75.0 - 80.0 min (45 - 100% of B), 80.0 -.90.0 (100 - 100% of B), 90.0 - 95 (100 - 35% of B). For the last three samples, the volume injection of 100 µL and flow rate of 8 mL/min was used.

3.4. Cytotoxicity Assay

The cytotoxicity of the ribifolones A-H was evaluated using the MTT (3-(4,5-dimethylthiazol-2-yl)-2,5-diphenyltetrazolium bromide) reduction assay [29]. SK-MEL-28 (human melanoma), HCT-116 (human colorectal carcinoma), and HEK-293 (non-tumor human embryonic kidney) cells were seeded in 96-well plates at densities of 1×10^5, 3×10^5 and 2×10^5 cells/mL, respectively. After a 24 h pre-incubation period to allow cell attachment, the cells were treated with ribifolones A-H at concentrations ranging from 1.56 to 100 µM and incubated for 72 h. Subsequently, MTT solution (5 mg/mL) was added to each well, and the plates were incubated for an additional 4 h at 37 °C and 5% of CO_2. The resulting formazan crystals were solubilized overnight with one hundred µL of 10% sodium dodecyl sulfate (SDS) solution [30]. Absorbance was measured at 570 nm using a microplate spectrophotometer. All experiments were performed in triplicate, and the half-maximal inhibitory concentration (IC_{50}) values were determined by nonlinear regression analysis using GraphPad Prism 8.0.1 software.

 doi:10.20944/preprints202603.1635.v1

3.5. Network Pharmacology

Initially, potential pharmacological targets for ribifolone C were collected using the AmIActive (AiA) and PharmMapper platforms [31,32]. Subsequently, the main targets involved in the onset and progression of colorectal and melanoma cancer were obtained through the GeneCards platform [33]. Next, the common targets between rib-3 and selected types of cancer were identified. These overlapping targets were used to construct two molecular interaction networks, one for colorectal cancer and the other for melanoma. For this purpose, the Search Tool for the Retrieval of Interacting Genes/Proteins (STRING) database was employed [34], considering a confidence score cutoff of 0.4 for protein–protein interactions.

The Cytoscape software (v. 3.10.3) was used for visualization and analysis of the constructed drug–disease networks [35]. Subsequently, functional enrichment analysis was performed to investigate the main signaling pathways associated with the common targets. For this, the protocol provided by the National Cancer Institute was followed, employing the clusterProfiler package in the R environment, focusing on the KEGG (Kyoto Encyclopedia of Genes and Genomes) category [36,37]. A significance criterion of $p < 0.05$ was adopted. Finally, the targets present in the main enriched pathways, as well as those described as relevant to the pathophysiology of melanoma and colorectal cancers, were selected for molecular docking and molecular dynamics studies.

3.6. Molecular Docking

Based *in vitro* assays, ribifolone C was selected to docking analysis, its structure was modeled using MarvinSketch v.25.3.0 software [23]. The targets were selected according to the highest number of interactions in the network analysis. Then, the crystallographic structures of four targets were obtained from the Protein Data Bank (PDB) (Table 1). Two compounds were used as standards for comparison, the cocrystallized inhibitor and the known active molecule jatrophone.

Table 6. This is a table. Tables should be placed in the main text near to the first time they are cited.

Targets	PDB (ID)	Resolution	Ligands	Reference
ERα*	1XP1	1.80 Å	Compound 15	[38]
ERβ**	1X76	2.20 Å	WAY-697	[39]
HER2***	3PP0	2.25 Å	SYR127063	[40]
HSP90α****	1UYF	2.00 Å	PU3	[41]
PI3Kγ*****	4HVB	2.35 Å	PF-04979064	[42]

*Human estrogen receptor alpha (ERα); **Human estrogen receptor beta (ERβ); ***Human Epidermal growth factor Receptor 2; ****Heat shock protein-90alpha; *****Phosphoinositide 3-kinase-γ.

Molegro Virtual Docker v.2013.6.0.1 was used to perform molecular docking [43]. All water molecules and cofactors were removed, and prior to molecular docking, a redocking step was carried out to assess the accuracy and reliability of the results using the Root-Mean-Square Deviation (RMSD), values ≤ 2 Å were considered satisfactory. The PI3K-Akt-mTOR pathway was analyzed using the PI3Kγ isoform, available in its cocrystallized form.

The simulation was conducted using default settings. The MolDock Score function was used to evaluate ligand poses, considering internal energy, hydrogen bonds, and torsional energy contributions. Fifty runs were performed using the MolDock SE algorithm, and the five best poses were retained. A grid with a radius of 15 Å and a resolution of 0.30 Å was generated, centered on the positions of the crystallographic ligands in the selected proteins. The docked poses were subsequently analyzed using Discovery Studio Visualizer v21.1.0.20298 [44].

Ligand Efficiency (LE) was calculated for all ligands [45]. Larger molecules tend to establish more contact points with the target, and therefore the docking score may reflect these multiple interactions rather than the intrinsic chemical efficiency of the molecule. LE is a metric in which the docking score is normalized by the number of heavy atoms, reflecting the actual effectiveness of the

 doi:10.20944/preprints202603.1635.v1

compound. LE was calculated according to Equation (1), where nHA denotes the number of heavy atoms.

$$\mathrm{LE} = \frac{\text{Docking score}}{\mathrm{nHA}}, \quad (1)$$

3.7. Molecular Dynamics

Molecular dynamics (MD) simulations were performed using GROMACS 5.0 [46] to evaluate the stability of the protein–ligand complexes. Ligand topologies were generated with the Automated Topology Builder (https://atb.uq.edu.au/index.py), applying the same force field as used for the protein, GROMOS54a7 [47].

Each system was solvated in a dodecahedron box of water molecules using the SPC extended point charge model, and sodium ions were added to neutralize the overall charge. Energy minimization was carried out to remove steric clashes, followed by equilibration in two stages. First, 100 ps of NVT equilibration was performed at 300 K using the velocity rescaling thermostat, followed by 100 ps of NPT equilibration at 1 atm using the Parrinello–Rahman barostat to stabilize the system. MD simulations were then performed for 200 ns with a timestep of 2 fs under periodic boundary conditions. The structural stability of the complexes was assessed by calculating the root mean square deviation (RMSD), while the flexibility of individual residues was evaluated using root mean square fluctuation (RMSF) analysis. The energy interaction of the protein-ligand complex was also calculated using the short-range Coulombic interaction energy and the Lennard-Jones short-range energy for 200 ns.

Ribifolone A (1)

Yellowish oil; UV (ACN) λmax 206, 213, 223, and 256 nm; IR (ATR) νmax 3529, 3406, 2961, 2929, 2877, 1754, 1651, cm^{-1}; ^{1}H and ^{13}C NMR data, see Table 1 and Table 2; positive-ion HR-ESI-MS *m/z* 345.1690 $[M - H_2O + H]^+$ (calcd for $C_{20}H_{25}O_5^+$, 345.1697, $\Delta_{m/z}$ theoretical = 2.0 ppm).

Ribifolone B (2)

Yellowish oil; UV (ACN) λmax 193, 208, 243, and 279 nm; IR (ATR) νmax 3458, 3363, 2938, 2923, 2868, 2854, 1706, 1683,1372,1054 cm^{-1}; ^{1}H and ^{13}C NMR data, see Table 1 and Table 2; positive-ion HR-ESI-MS *m/z* 347.1857 $[M - H_2O + H]^+$ (calcd for $C_{20}H_{26}O_5^+$, 347.1853, $\Delta_{m/z}$ theoretical = -1.3 ppm).

Ribifolone C (3)

White amorphous powder; UV (ACN) λmax 201, 219, 247, and 279 nm; IR (ATR) νmax 2964, 2941, 2895, 1746, 1691, 1223, 1036 cm^{-1}; ^{1}H and ^{13}C NMR data, see Table 1 and Table 2; positive-ion HR-ESI-MS *m/z* 351.1572 $[M + Na]^+$ (calcd for $C_{20}H_{24}NaO_4$, 351.1567, $\Delta_{m/z}$ theoretical = -1.6 ppm).

Ribifolone D (4)

Yellowish oil; UV (ACN) λmax 218 and 277 nm; IR (ATR) νmax 3420, 2961, 2929, 2872, 1697, 1622, 1370 cm^{-1}; ^{1}H and ^{13}C NMR data, see Table 1 and Table 2; positive-ion HR-ESI-MS *m/z* 311.1632 $[M - H_2O + H]^+$ (calcd. for $C_{20}H_{23}O_3^+$, 311.1642, $\Delta_{m/z}$ theoretical = 3.3 ppm).

Ribifolone E (5)

Yellow oil; UV (ACN) λmax 216 and 278 nm; IR (ATR) νmax 2958, 2926, 2872, 1703, 1619, cm^{-1}; ^{1}H and ^{13}C NMR data, see Table 1 and Table 2; positive-ion HR-ESI-MS *m/z* 311.1637 $[M+H]^+$ (calcd for $C_{20}H_{23}O_3^+$; 311.1642, $\Delta_{m/z}$ theoretical = 1.5 ppm ppm).

Ribifolone F (6)

White amorphous powder; UV (ACN) λmax 193,237 and 245 nm; IR (ATR) νmax 3015, 2964, 2877, 1749, 1691, 1223, 1042 cm^{-1}; ^{1}H and ^{13}C NMR data, see Table 1 and Table 2; positive-ion HR-ESI-MS *m/z* 331.1903 $[M + H]^+$ (calcd for $C_{20}H_{27}O_4^+$, $\Delta_{m/z}$ theoretical = 0.1 ppm).

Ribifolone G (7)

Yellowish oil; UV (ACN) λmax 193, 225 and 282 nm; IR (ATR) νmax 3437, 2958, 2926, 2872, 1746, 1235, 1077 cm^{-1}; ^{1}H and ^{13}C NMR data, see Table 1 and Table 2; positive-ion HR-ESI-MS *m/z* 313.1798 $[M - H_2O + H]^+$ (calcd for $C_{20}H_{25}O_3^+$, 313.1798, $\Delta_{m/z}$ theoretical = 1.4 ppm).

Ribifolone H (8)

 doi:10.20944/preprints202603.1635.v1

Yellowish oil; UV (ACN) λmax 200, 225, 273, and 394 nm; IR (ATR) νmax 3630, 3413, 3235, 1638, 1617, 1562, 1384, 621 cm^{-1}; ^{1}H and ^{13}C NMR data, see Table 1 and Table 2; positive-ion HR-ESI-MS *m/z* 369.1672 $[M + Na]^+$ (calcd for $C_{20}H_{26}NaO_5^+$, 369.1672, Δ*m/z* theoretical = 0.1 ppm).

4. Conclusions

The chemical and biological investigation of *J. ribifolia* led to the isolation and structural characterization of sixteen compounds, including eight new macrocyclic diterpenes, herein named ribifolones A–H. Ribifolones A, C and D exhibited cytotoxic effects against melanoma (SK-MEL-28) and colorectal cancer (HCT-116) cell lines, although with distinct potency profiles. Among the series, ribifolone C and jatrophone displayed comparatively stronger activity. Ribifolone C showed IC_{50} values of 50.71 μM and 33.39 μM, whereas jatrophone presented IC_{50} values of 6.19 μM and 10.09 μM against SK-MEL-28 and HCT-116 cells, respectively. Although the cytotoxic activity of jatrophone is consistent with its previously reported antitumor profile, the effects observed for ribifolones indicate the potential of jatrophane diterpenes as a promising scaffold for future optimization. The complementary application of network pharmacology, molecular docking, and molecular dynamics simulations provided mechanistic indications that both compounds may modulate the PI3K–AKT signaling pathway, with estrogen receptor beta (ERβ) emerging as a putative target. Nevertheless, these *in silico* findings require further experimental validation to confirm the proposed molecular interactions and downstream biological effects.

In summary, these findings highlight the chemical diversity of the *Jatropha* genus and reinforce the pharmacological relevance of *J. ribifolia*. The integration of *in vitro* and *in silico* strategies proved valuable for generating biologically grounded hypotheses, supporting the continued exploration of *Euphorbiaceae* species as sources of structurally distinctive bioactive metabolites.

Supplementary Materials: The following supporting information can be downloaded at: Preprints.org.

Author Contributions: Conceptualization, T.A.S.; Writing original draft preparation, T.A.S. and A.F.A.; Writing – review and editing, M.T.S, L.S.A.; Methodology, M.F.A; M.T.S; L.S.; R.R.M.S.; M.V.A. and T.A.M.B.; Formal analysis, A.C.F.A.; F.M.S; L.S. and M.T.S.; Project administration, J.F.T.; Supervision and Funding acquisition, M.S.S. All authors have read and agreed to the published version of the manuscript

Funding: This work was supported by Coordenação de Aperfeiçoamento do Pessoal de Nível Superior (CAPES, Finance Code 001) and Fianciadora de Estudos e Projetos (FINEP) by means of INCT-RENNOFITO.

Institutional Review Board Statement: Not applicable.

Acknowledgments: The authors thanks the Conselho Nacional de Desenvolvimento Científico e Tecnológico (CNPq), grant numbers 302469/2022-2, 152472/2024-0 and 306633/2021-3. Fundação de Amparo à Pesquisa do Estado do Rio de Janeiro (FAPERJ), grant number E-26/210–313/2022.

Conflicts of Interest: The authors declare no conflicts of interest.

Abbreviations

The following abbreviations are used in this manuscript:

MDPI	Multidisciplinary Digital Publishing Institute
DOAJ	Directory of open access journals
TLA	Three letter acronyms
LD	Linear dichroism

References

1. Cavalcante, N.B.; Diego da Conceição Santos, A.; Guedes da Silva Almeida, J.R. The Genus Jatropha (Euphorbiaceae): A Review on Secondary Chemical Metabolites and Biological Aspects. *Chem. Biol. Interact.* **2020**, *318*, 108976, doi:10.1016/j.cbi.2020.108976.

 doi:10.20944/preprints202603.1635.v1

2. Agra, M. de F.; Freitas, P.F. de; Barbosa-Filho, J.M. Synopsis of the Plants Known as Medicinal and Poisonous in Northeast of Brazil. *Revista Brasileira de Farmacognosia* **2007**, *17*, 114–140, doi:10.1590/S0102-695X2007000100021.
3. Pinto, M.E.F.; Batista, J.M.; Koehbach, J.; Gaur, P.; Sharma, A.; Nakabashi, M.; Cilli, E.M.; Giesel, G.M.; Verli, H.; Gruber, C.W.; et al. Ribifolin, an Orbitide from *Jatropha Ribifolia* , and Its Potential Antimalarial Activity. *J. Nat. Prod.* **2015**, *78*, 374–380, doi:10.1021/np5007668.
4. Fernandes, E. de S.; Rodrigues, F.A.; Tófoli, D.; Imamura, P.M.; de Carvalho, J.E.; Ruiz, A.L.T.G.; Foglio, M.A.; Minguzzi, S.; Silva, R.C.L. Isolation, Structural Identification and Cytotoxic Activity of Hexanic Extract, Cyperenoic Acid, and Jatrophone Terpenes from Jatropha Ribifolia Roots. *Revista Brasileira de Farmacognosia* **2013**, *23*, 441–446, doi:10.1590/S0102-695X2013005000026.
5. A. de Souza, T.; F. Alves, A.; D. T. Lira, N.; P. Cibulski, S.; H. A. Pereira, L.; S. Abreu, L.; F. Tavares, J.; T. Scotti, M.; S. da Silva, M. Chemotaxonomic Analysis of Diterpenes in Four Euphorbiaceae Genera: A Path to New Cytotoxic Agents. *J. Braz. Chem. Soc.* **2025**, doi:10.21577/0103-5053.20250061.
6. Liu, Y.; Zhang, S.; Liu, K.; Hu, X.; Gu, X. Advances in Drug Discovery Based on Network Pharmacology and Omics Technology. *Curr. Pharm. Anal.* **2024**, *21*, 33–43, doi:10.1016/j.cpan.2024.12.002.
7. Li, L.; Kar, S. Leveraging Network Pharmacology for Drug Discovery: Integrative Approaches and Emerging Insights. *Med. Drug Discov.* **2025**, *27*, 100220, doi:10.1016/j.medidd.2025.100220.
8. Zhou, Z.; Chen, B.; Chen, S.; Lin, M.; Chen, Y.; Jin, S.; Chen, W.; Zhang, Y. Applications of Network Pharmacology in Traditional Chinese Medicine Research. *Evidence-Based Complementary and Alternative Medicine* **2020**, *2020*, doi:10.1155/2020/1646905.
9. Yang, J.; Long, Y.O.; Paquette, L.A. Concise Total Syntheses of the Bioactive Mesotricyclic Diterpenoids Jatrophatrione and Citlalitrione. *J. Am. Chem. Soc.* **2003**, *125*, 1567–1574, doi:10.1021/ja021177r.
10. Pertino, M.; Schmeda-Hirschmann, G.; Rodríguez, J.A.; Theoduloz, C. Gastroprotective Effect and Cytotoxicity of Terpenes from the Paraguayan Crude Drug "Yagua Rova" (Jatropha Isabelli). *J. Ethnopharmacol.* **2007**, *111*, 553–559, doi:10.1016/j.jep.2007.01.003.
11. Taylor, M.D.; Smith, A.B.; Furst, G.T.; Gunasekara, S.P.; Bevelle, C.A.; Cordell, G.A.; Farnsworth, N.R.; Kupchan, S.M.; Uchida, H. Plant Anticancer Agents. 28. New Antileukemic Jatrophone Derivatives from Jatropha Gossypiifolia: Structural and Stereochemical Assignment through Nuclear Magnetic Resonance Spectroscopy. *J. Am. Chem. Soc.* **1983**, *105*, 3177–3183, doi:10.1021/ja00348a036.
12. Kanth, B.S.; Kumar, A.S.; Shinde, D.B.; Babu, K.H.; Raju, T.V.; Kumar, C.G.; Sujitha, P.; Das, B. New Bioactive Macrocyclic Diterpenoids from Jatropha Multifida. *Bioorg. Med. Chem. Lett.* **2011**, *21*, 6808–6810, doi:10.1016/j.bmcl.2011.09.032.
13. Taylor, M.D.; Smith, A.B.; Furst, G.T.; Gunasekara, S.P.; Bevelle, C.A.; Cordell, G.A.; Farnsworth, N.R.; Kupchan, S.M.; Uchida, H. Plant Anticancer Agents. 28. New Antileukemic Jatrophone Derivatives from Jatropha Gossypiifolia: Structural and Stereochemical Assignment through Nuclear Magnetic Resonance Spectroscopy. *J. Am. Chem. Soc.* **1983**, *105*, 3177–3183, doi:10.1021/ja00348a036.
14. Indrayanto, G.; Putra, G.S.; Suhud, F. Validation of In-Vitro Bioassay Methods: Application in Herbal Drug Research. In *Profiles of Drug Substances, Excipients and Related Methodology*; 2021; pp. 273–307.
15. Fattahian, M.; Ghanadian, M.; Ali, Z.; Khan, I.A. Jatrophane and Rearranged Jatrophane-Type Diterpenes: Biogenesis, Structure, Isolation, Biological Activity and SARs (1984–2019). *Phytochemistry Reviews* **2020**, *19*, 265–336, doi:10.1007/s11101-020-09667-8.
16. Lu, Y.-B.; Luo, S.; Wang, Y.-X.; Feng, Z.-Y.; Gao, K.; Chen, J.-J. Jatrophane Diterpenoids with Cytotoxic Activity from the Whole Plant of Euphorbia Heliosocpia L. *Phytochemistry* **2022**, *203*, 113420, doi:10.1016/j.phytochem.2022.113420.
17. Pešić, M.; Banković, J.; Aljančić, I.S.; Todorović, N.M.; Jadranin, M.; Vajs, V.E.; Tešević, V. V.; Vučković, I.; Momčilović, M.; Marković, I.D.; et al. New Anti-Cancer Characteristics of Jatrophane Diterpenes from Euphorbia Dendroides. *Food and Chemical Toxicology* **2011**, *49*, 3165–3173, doi:10.1016/j.fct.2011.09.035.
18. Souza, T.A. de; Pereira, L.H.A.; Alves, A.F.; Dourado, D.; Lins, J. da S.; Scotti, M.T.; Scotti, L.; Abreu, L.S.; Tavares, J.F.; Silva, M.S. Jatropha Diterpenes: An Updated Review Concerning Their Structural Diversity, Therapeutic Performance, and Future Pharmaceutical Applications. *Pharmaceuticals* **2024**, *17*, 1399, doi:10.3390/ph17101399.

 doi:10.20944/preprints202603.1635.v1

19. Jiang, M.; Zhang, K.; Zhang, Z.; Zeng, X.; Huang, Z.; Qin, P.; Xie, Z.; Cai, X.; Ashrafizadeh, M.; Tian, Y.; et al. PI3K/AKT/MTOR Axis in Cancer: From Pathogenesis to Treatment. *MedComm (Beijing).* **2025**, *6*, doi:10.1002/mco2.70295.
20. Glaviano, A.; Foo, A.S.C.; Lam, H.Y.; Yap, K.C.H.; Jacot, W.; Jones, R.H.; Eng, H.; Nair, M.G.; Makvandi, P.; Geoerger, B.; et al. PI3K/AKT/MTOR Signaling Transduction Pathway and Targeted Therapies in Cancer. *Mol. Cancer* **2023**, *22*, 138, doi:10.1186/s12943-023-01827-6.
21. Paggi, J.M.; Pandit, A.; Dror, R.O. The Art and Science of Molecular Docking. *Annu. Rev. Biochem.* **2024**, *93*, 389–410, doi:10.1146/annurev-biochem-030222-120000.
22. Chen, P.; Li, B.; Ou-Yang, L. Role of Estrogen Receptors in Health and Disease. *Front. Endocrinol. (Lausanne).* **2022**, *13*, doi:10.3389/fendo.2022.839005.
23. Treneff, J.; McCrary, A.; Burd, C. Abstract 4055: Estrogen Receptor Beta Suppresses Melanoma Progression through Modulation of Melanocyte Master Regulator Activity. *Cancer Res.* **2025**, *85*, 4055–4055, doi:10.1158/1538-7445.AM2025-4055.
24. Das, P.K.; Saha, J.; Pillai, S.; Lam, A.K. -Y.; Gopalan, V.; Islam, F. Implications of Estrogen and Its Receptors in Colorectal Carcinoma. *Cancer Med.* **2023**, *12*, 4367–4379, doi:10.1002/cam4.5242.
25. Rawłuszko-Wieczorek, A.A.; Lipowicz, J.; Nowacka, M.; Ostrowska, K.; Pietras, P.; Blatkiewicz, M.; Ruciński, M.; Jagodziński, P.P.; Nowicki, M. Estrogen Receptor β Affects Hypoxia Response in Colorectal Cancer Cells. *Biochimica et Biophysica Acta (BBA) - Molecular Basis of Disease* **2024**, *1870*, 166894, doi:10.1016/j.bbadis.2023.166894.
26. Mori, T.; Martinez, S.R.; O'Day, S.J.; Morton, D.L.; Umetani, N.; Kitago, M.; Tanemura, A.; Nguyen, S.L.; Tran, A.N.; Wang, H.-J.; et al. Estrogen Receptor-α Methylation Predicts Melanoma Progression. *Cancer Res.* **2006**, *66*, 6692–6698, doi:10.1158/0008-5472.CAN-06-0801.
27. Roney, M.; Mohd Aluwi, M.F.F. The Importance of In-Silico Studies in Drug Discovery. *Intelligent Pharmacy* **2024**, *2*, 578–579, doi:10.1016/j.ipha.2024.01.010.
28. Shah, A.; Jain, M. Limitations and Future Challenges of Computer-Aided Drug Design Methods. In *Computer Aided Drug Design (CADD): From Ligand-Based Methods to Structure-Based Approaches*; Elsevier, 2022; pp. 283–297.
29. Mosmann, T. Rapid Colorimetric Assay for Cellular Growth and Survival: Application to Proliferation and Cytotoxicity Assays. *J. Immunol. Methods* **1983**, *65*, 55–63, doi:10.1016/0022-1759(83)90303-4.
30. Sousa, V.M. de; Duarte, S.S.; Ferreira, R.C.; Sousa, N.F. de; Scotti, M.T.; Scotti, L.; Silva, M.S. da; Tavares, J.F.; Moura, R.O. de; Gonçalves, J.C.R.; et al. AMTAC-19, a Spiro-Acridine Compound, Induces In Vitro Antitumor Effect via the ROS-ERK/JNK Signaling Pathway. *Molecules* **2024**, *29*, 5344, doi:10.3390/molecules29225344.
31. de Morais Melo, L.F.; de Oliveira Filho, L.P.; Ferreira, U. de A.; Pessoa Alves, E.H.; Oliveira Costa, R.P.; Scotti, L.; Scotti, M.T. AmIActive (AIA): A Large-Scale QSAR Based Target Fishing and Polypharmacology Predictive Web Tool. *J. Mol. Biol.* **2025**, *437*, 169090, doi:10.1016/j.jmb.2025.169090.
32. Wang, X.; Shen, Y.; Wang, S.; Li, S.; Zhang, W.; Liu, X.; Lai, L.; Pei, J.; Li, H. PharmMapper 2017 Update: A Web Server for Potential Drug Target Identification with a Comprehensive Target Pharmacophore Database. *Nucleic Acids Res.* **2017**, *45*, W356–W360, doi:10.1093/nar/gkx374.
33. Stelzer, G.; Rosen, N.; Plaschkes, I.; Zimmerman, S.; Twik, M.; Fishilevich, S.; Stein, T.I.; Nudel, R.; Lieder, I.; Mazor, Y.; et al. The GeneCards Suite: From Gene Data Mining to Disease Genome Sequence Analyses. *Curr. Protoc. Bioinformatics* **2016**, *54*, doi:10.1002/cpbi.5.
34. Szklarczyk, D.; Franceschini, A.; Wyder, S.; Forslund, K.; Heller, D.; Huerta-Cepas, J.; Simonovic, M.; Roth, A.; Santos, A.; Tsafou, K.P.; et al. STRING V10: Protein-Protein Interaction Networks, Integrated over the Tree of Life. *Nucleic Acids Res.* **2015**, *43*, D447-52, doi:10.1093/nar/gku1003.
35. Shannon, P.; Markiel, A.; Ozier, O.; Baliga, N.S.; Wang, J.T.; Ramage, D.; Amin, N.; Schwikowski, B.; Ideker, T. Cytoscape: A Software Environment for Integrated Models of Biomolecular Interaction Networks. *Genome Res.* **2003**, *13*, 2498–2504, doi:10.1101/gr.1239303.
36. Kanehisa, M. The KEGG Database. *Novartis Found. Symp.* **2002**, *247*, 91–101; discussion 101-3, 119–128, 244–252.

 doi:10.20944/preprints202603.1635.v1

37. Wu, T.; Hu, E.; Xu, S.; Chen, M.; Guo, P.; Dai, Z.; Feng, T.; Zhou, L.; Tang, W.; Zhan, L.; et al. ClusterProfiler 4.0: A Universal Enrichment Tool for Interpreting Omics Data. *Innovation (Cambridge (Mass.))* **2021**, *2*, 100141, doi:10.1016/j.xinn.2021.100141.
38. Blizzard, T.A.; DiNinno, F.; Morgan, J.D.; Chen, H.Y.; Wu, J.Y.; Kim, S.; Chan, W.; Birzin, E.T.; Yang, Y.T.; Pai, L.-Y.; et al. Estrogen Receptor Ligands. Part 9: Dihydrobenzoxathiin SERAMs with Alkyl Substituted Pyrrolidine Side Chains and Linkers. *Bioorg. Med. Chem. Lett.* **2005**, *15*, 107–113, doi:10.1016/j.bmcl.2004.10.036.
39. Manas, E.S.; Unwalla, R.J.; Xu, Z.B.; Malamas, M.S.; Miller, C.P.; Harris, H.A.; Hsiao, C.; Akopian, T.; Hum, W.-T.; Malakian, K.; et al. Structure-Based Design of Estrogen Receptor-β Selective Ligands. *J. Am. Chem. Soc.* **2004**, *126*, 15106–15119, doi:10.1021/ja047633o.
40. Aertgeerts, K.; Skene, R.; Yano, J.; Sang, B.-C.; Zou, H.; Snell, G.; Jennings, A.; Iwamoto, K.; Habuka, N.; Hirokawa, A.; et al. Structural Analysis of the Mechanism of Inhibition and Allosteric Activation of the Kinase Domain of HER2 Protein. *Journal of Biological Chemistry* **2011**, *286*, 18756–18765, doi:10.1074/jbc.M110.206193.
41. Wright, L.; Barril, X.; Dymock, B.; Sheridan, L.; Surgenor, A.; Beswick, M.; Drysdale, M.; Collier, A.; Massey, A.; Davies, N.; et al. Structure-Activity Relationships in Purine-Based Inhibitor Binding to HSP90 Isoforms. *Chem. Biol.* **2004**, *11*, 775–785, doi:10.1016/j.chembiol.2004.03.033.
42. Cheng, H.; Li, C.; Bailey, S.; Baxi, S.M.; Goulet, L.; Guo, L.; Hoffman, J.; Jiang, Y.; Johnson, T.O.; Johnson, T.W.; et al. Discovery of the Highly Potent PI3K/MTOR Dual Inhibitor PF-04979064 through Structure-Based Drug Design. *ACS Med. Chem. Lett.* **2013**, *4*, 91–97, doi:10.1021/ml300309h.
43. CLC BIO COMPANY. Molegro Virtual Docker, Versão 6.0.1 [Software] 2013.
44. Dassault Systèmes Discovery Studio Visualizer, V21.1.0.20298. [Software] 2019.
45. Jabeen, I.; Pleban, K.; Rinner, U.; Chiba, P.; Ecker, G.F. Structure–Activity Relationships, Ligand Efficiency, and Lipophilic Efficiency Profiles of Benzophenone-Type Inhibitors of the Multidrug Transporter P-Glycoprotein. *J. Med. Chem.* **2012**, *55*, 3261–3273, doi:10.1021/jm201705f.
46. Abraham, M.J.; Murtola, T.; Schulz, R.; Páll, S.; Smith, J.C.; Hess, B.; Lindahl, E. GROMACS: High Performance Molecular Simulations through Multi-Level Parallelism from Laptops to Supercomputers. *SoftwareX* **2015**, *1–2*, 19–25, doi:10.1016/j.softx.2015.06.001.
47. Schmid, N.; Eichenberger, A.P.; Choutko, A.; Riniker, S.; Winger, M.; Mark, A.E.; van Gunsteren, W.F. Definition and Testing of the GROMOS Force-Field Versions 54A7 and 54B7. *European Biophysics Journal* **2011**, *40*, 843–856, doi:10.1007/s00249-011-0700-9.